Materials Research. 2023; 26(suppl. 1): e20220492
DOI: https://doi.org/10.1590/1980-5373-MR-2022-0492

Production of Polycaprolactone/Atorvastatin Films for Drug Delivery Application

Debora Baptista Pereira[a]*, Beatriz Ferreira de Carvalho Patricio[b,c,d], Talita Goulart da Silva[a], Hellen Regina Oliveira de Almeida[a], Marcelo Henrique da Cunha Chaves[b,c], Michelle Alvares Sarcinelli[b,c], Helvécio Vinícius Antunes Rocha[b,c], Tiago dos Santos Mendonça[e], Tiago José Bandeira Sales[a], Roberta Helena Mendonça[a,c]

[a]Universidade Federal Rural do Rio de Janeiro, Instituto de Tecnologia, Departamento de Engenharia Química, Seropédica, RJ, Brasil.
[b]Instituto de Tecnologia Farmacêutica (Farmanguinhos), Laboratório de Micro e Nanotecnologia, Brasil.
[c]Fundação Carlos Chagas Filho de Amparo à Pesquisa do Estado do Rio de Janeiro (FAPERJ), Rede de Inovação em Nanosistemas para a Saúde (NanoSAÚDE), Rio de Janeiro, RJ, Brasil.
[d]Universidade Federal do Estado do Rio de Janeiro (UNIRIO), Instituto Biomédico, Departamento de Ciências Fisiológicas, Rio de Janeiro, RJ, Brasil.
[e]Universidade Estadual do Rio de Janeiro, Instituto de Física A.D. Tavares, Departamento de Física Teórica, Rua São Francisco Xavier, 524, 20550-013, Rio de Janeiro, RJ, Brasil.

Received: November 22, 2022; Revised: March 24, 2023; Accepted: May 03, 2023

Developing biomaterials for tissue regeneration is a promising alternative for the recovery of various tissues, including bone. Atorvastatin (ATV) has a series of beneficial effects which includes bone anabolism, vasodilating, and anti-inflammatory actions. The main objective of this work was to produce and characterize polycaprolactone (PCL) matrices incorporated with ATV. Samples were prepared by the solvent casting technique. Scanning electron microscopy (SEM), X-Ray diffraction (XRD), Fourier transform infrared spectrometry (FTIR), thermogravimetric analysis (TGA), differential scanning calorimetry (DSC) and *in vitro* release studies were performed. FTIR analysis showed that no chemical bonds were formed between PCL and ATV. SEM analysis showed that the amount of ATV affects sample morphology. According to XRD and thermal analysis, the main ATV characteristics were maintained. The studies showed that PCL/ATV samples release the drug in a prolonged way since its release reaches around 50% after 15000 minutes of analysis and the model that showed the best fit for the studied matrices was the Higuchi model, with a correlation coefficient above 0.95.

Keywords: *Atorvastatin, biomaterials, bioengineering, drug release, polymeric matrices.*

1. Introduction

Atorvastatin (ATV) belongs to the pharmacological class of statins and is an anti-cholesterol drug that inhibits the HMG-CoA reductase, an essential enzyme in cholesterol synthesis, and reduces cholesterol production by the human organism[1]. Traditionally, this drug is presented as a tablet. It has an absorbed fraction and absolute bioavailability of about 30% and 12%, respectively, due to a pre-systemic clearance in the gastrointestinal mucosa and its first-pass hepatic metabolism[2,3]. However, ATV has beneficial effects unrelated to lipid metabolism, the so-called pleiotropic effects. This includes bone anabolism, vasodilating, antithrombotic, antioxidant, anti-inflammatory, and immunosuppressive actions[4,5]. In 2002, Pasco et al.[6], in a retrospective case-control study, Statins were associated with a 60% reduction in the risk of bone fractures when evaluating 1,375 women aged 50 to 95 years[6]. Some statins have been studied with polymers for controlled release[7,8]. However, for ATV, there is still no study available.

Biodegradable polymers have been investigated as raw materials to manufacture biomaterials applied to tissue regeneration and devices for drug delivery[9-14]. Due to Polycaprolactone (PCL) biocompatibility, and biodegradability, several applications in the medical field are found for it, such as drug delivery systems[9,15]; films applied to tissue-engineered skin[16-18]; coating for urethral stents in musculoskeletal tissue engineering[19] and scaffolds for supporting osteoblast and fibroblast growth[19,20] microspheres and nano formulations for drug delivery applied to cancer treatment[21]; and resorbable scaffolds by injection molding for application in orbital eye repair[22].

Mainly, PCL has been extensively studied to produce materials applied to both bone and cartilage repair[19,22,23]. In this context, different techniques such as electrospinning, solvent casting, and compression molding, among others[9,22], have been used to produce biomaterials in different formats, such as films[9], scaffolds[9], among others[24].

Biomaterials have played a prominent role in the development of tissue regeneration[1]. It can be used for local drug delivery

*e-mail: debora.d94@hotmail.com

as a promising alternative to recover various tissues, including bone[1]. In this context, two different technologies, the controlled release of drugs and tissue engineering, can be combined to provide efficient results in tissue repair. Polymeric materials in matrices, films, or scaffolds can guide and support tissue regeneration and work as vehicles for drug delivery[9-13]. The technology of controlled release of drugs can potentially overpass many problems related to the traditional administration of active pharmaceutical ingredients by regulating the rate and spatial localization of the released agent[14].

Recent studies on metabolic abnormalities and obesity, particularly abnormal lipid metabolism, have been associated with diseases caused by cartilage degeneration, such as osteoarthritis[25]. Developing materials based on PCL and ATV can be an alternative to treat problems associated with bone, local cholesterol disorder, and cartilage diseases due to PCL[9,10] and ATV characteristics[25,26]. Thus, the objective of the present work was to produce and characterize PCL/ATV matrices with prolonged drug release.

2. Experimental

2.1 . Materials

Atorvastatin calcium was kindly donated by the Oswaldo Cruz Foundation. PCL (average molar mass of 60,000g/mol) was supplied by Polymorph Ltd, China. Chloroform (PA) was obtained from Labsynth, Brazil. The manufacturer's name will not be disclosed for confidentiality reasons.

2.2. Production of PCL/ATV matrices

The polymeric matrices were prepared by solvent casting, where atorvastatin calcium and PCL were solubilized in 2 mL of chloroform at room temperature using room temperature the following quantity of atorvastatin 0; 0.1; 0.2; and 0.4 mg ATV/mg PCL. The values were based on the ATV pill formulations. The resulting mixtures were added to silicone molds (3 cm x 2 cm) and dried at room temperature for 1 hour. The matrices were named according to the amount of ATV in the sample: PCL (0 mg of ATV), PA20 (20 mg of ATV); PA40 (40 mg of ATV); PA60 (60 mg of ATV); PA80 (80 mg of ATV).

2.3. Fourier-Transform Infrared Spectroscopy (FTIR)

FTIR analysis was performed to investigate the possible interactions between ATV and PCL. The analysis was done using an Infrared Spectrometer (Bruker, model Vertex 7) with attenuated total reflectance (ATR) by recording measurements from 4000 to 400 cm^{-1} and 64 scans and compared with the raw materials (PCL and ATV).

2.4. X-Ray Diffraction (XRD)

All the samples were analyzed on an X-Ray diffractometer (Rigaku, model Mini Flex II) operated with the Cukα source ($\lambda = 1.5418$ Å). The scans were recorded over the $2\theta = 6–60°$, with a 2°/min scan speed.

2.5. Thermogravimetric analysis (TGA)

PCL, ATV, PA20, PA40, PA60, and PA80 samples were analyzed on a thermogravimetric analyzer (model Discovery 550, TA Instruments). The measurement was performed using platinum pans with about 5 mg of the sample at a heating rate of 20 °C/min under a nitrogen atmosphere, from room temperature to 700 °C. TGA curves and their derivative (DTG) were obtained.

2.6. Differential Scanning Calorimetry (DSC)

PCL, ATV, PA20, PA40, PA60, and PA80 samples were characterized on a differential scanning calorimeter (DSC model Discovery 250, TA Instruments). Samples with a mass of around 5 mg were heated in aluminum pans in the range from room temperature to 300°C, with a heating rate of 10°C/min under a flowing dry nitrogen atmosphere (20 cm^3/min).

2.7. Scanning Electron Microscopy (SEM) and Energy Dispersive Spectroscopy (EDS)

To evaluate the morphology of the samples with different amounts of ATV, the raw materials, PA20, PA40, PA60, and PA80 samples were analyzed using a scanning electron microscope (JEOL, model JSM-6390LV) at an acceleration voltage of 15 kV. For this analysis, samples were recovered with gold.

The samples were vaporized with carbon to observe the drug distribution on the matrices, and an EDS spectrum was acquired. The spectra acquisition was made for 30 sec with a 15kV and 79 mA beam at 10 mm and a spot size of 71. For the acquisition of the EDS map, the exact condition of the beam was used, and it acquired 500 frames with a dead time between 17-19%.

2.8. In vitro release studies

To evaluate the capacity of the prepared films in releasing ATV, they were submitted to an in vitro release study using UV-Vis. A standard curve of ATV in a phosphate medium was obtained at 240 nm. Therefore, the in vitro release study was conducted using a Distek Evolution 6100 dissolution test system. The experiment was done in triplicate, using three vats for each sample. The samples (PA20 and PA40) were immersed in 900 mL of potassium phosphate buffer (pH = 7.4), at 37°C, under the agitation of 75 rpm, and aliquots were withdrawn at the following predetermined intervals: 5, 30, 60, 90, 120, 150, 180, 210, 240, 1440, 1800, 2880, 3180, 4320, 5760, 5940, 10080, 11520, 12960, 14400 and 15840 min. The drug concentrations were calculated using the equation ($y = 33.195x + 0.0176$; with a correlation coefficient of 0.9603) obtained through the analytical curve of ATV in phosphate buffer pH 7.4. Drug releases were adjusted for the following models: zero-order kinetics, first order-kinetics, Hixson-Crowell, Higuchi, and Korsmeyer-Peppas[27,28]. The linearity of the results was evaluated by the determination coefficients (R^2). After the *in vitro* release study, the matrices morphology was analyzed by SEM as described in the above section.

3. Results and discussion

3.1. FTIR analysis

FTIR analysis of PCL, ATV, and samples containing different amounts of ATV was performed, and the spectra are shown in Figure 1. The prominent bands of PCL and ATV are also presented in Figure 1. The results showed that

ATV and PCL present bands with wavenumbers closer than those reported in the literature[19,29-31].

The spectra of PA20, PA40, PA60, and PA80 samples present the characteristic bands of both pure PCL and pure ATV. With the increase in the proportion of ATV in the samples, the ATV bands become more evident (Figure 1). The ATV characteristic bands around 1646 cm^{-1} for (C = O) and 1575 cm^{-1} for (C - N) can be observed in the region ranging from 1900 cm^{-1} to 1350 cm^{-1}. The strong carbonyl absorption of PCL overlaps the carbonyl absorption bands of ATV. Therefore, according to FTIR analyses, no chemical linkage was formed between ATV and PCL, and this is important as the primary objective is the release of ATV.

3.2. XRD analysis

PCL matrix, ATV, and PCL/ATV samples were analyzed by XRD and the diffractograms are shown in Figure 2. The diffractogram of PCL (See in detail on the left side in Figure 2) presented characteristic peaks at 2(θ) equal to: 22.2° and 25.2°. In the diffractogram of ATV See in detail on the right side in Figure 2), the main peaks were observed at: 2θ = 9.24° e 9.59°; 2θ = 10.37°; 2θ = 11.96° e 12.30°, 2θ = 17.05°; 2θ = 19.57°; 2θ = 21.65° and 2θ = 23.81°.

The peaks related to PCL and ATV were observed in the samples PA20, PA40, PA60, and PA80. Peaks related to ATV, as in 2θ = 17.05° and 2θ = 19.57° are more clearly observed in samples with a greater amount of the drug[3,32] (See in detail on the right side in Figure 2). According to Figure 2, changes in PCL pick position occurred, probably due to the presence of ATV.

3.3. Thermal analysis - DSC, TGA and DTG

The samples PA20, PA40, PA60, PA80, PCL, and ATV were analyzed by TGA and DSC to evaluate the thermal properties of these materials. DTG results are presented in Table 1. DSC curves are shown in Figure 3 and the Endothermic events values in Table 2.

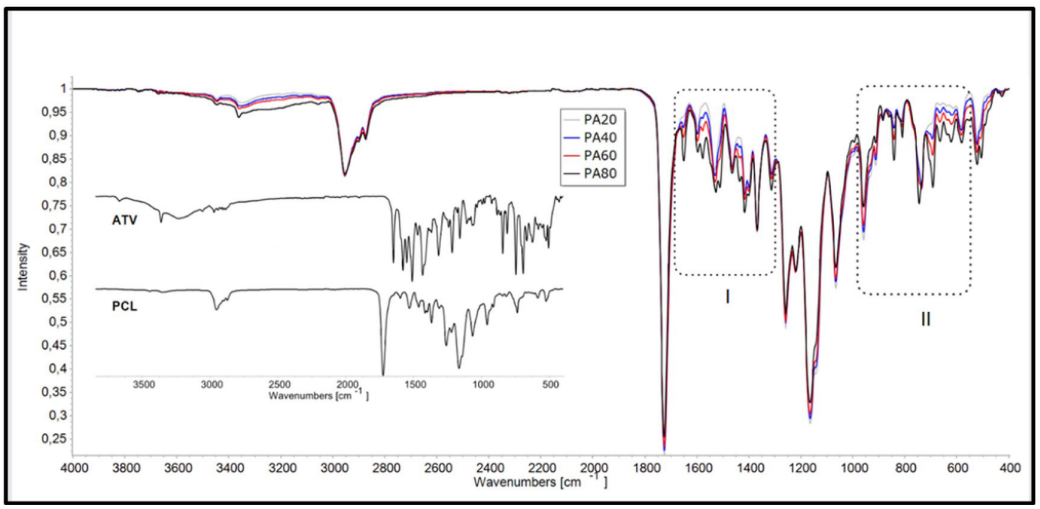

Figure 1. FTIR spectra of the matrices - PCL (0 mg of ATV); PA20 (20 mg of ATV); PA40 (40 mg of ATV); PA60 (60 mg of ATV); PA80 (80 mg of ATV); and ATV.

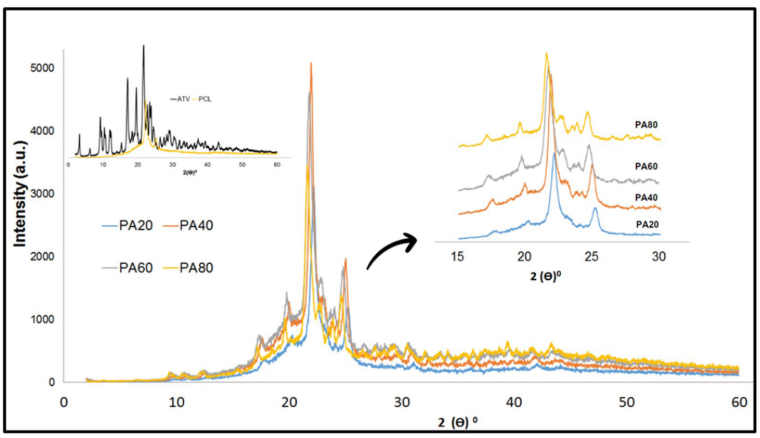

Figure 2. Diffractograms of the matrices: PCL (0 mg of ATV), PA20 (20 mg of ATV); PA40 (40 mg of ATV); PA60 (60 mg of ATV); PA80 (80 mg of ATV); and ATV.

Table 1. DTG maximum values for ATV, PCL, and PCL/ATV samples.

Samples	The first step of degradation T_{max} (°C)	The second step of degradation T_{max} (°C)	The third step of degradation T_{max} (°C)	The fourth step of degradation T_{max} (°C)	The fifth step of degradation T_{max} (°C)
PA20	254.96	376.27	417.64	451.57	-
PA40	252.17	333.52	430.27	484.54	-
PA60	250.30	347.92	427.98	473.88	643.07
PA80	252.39	352.28	419.43	465.72	624.24
ATV	251.40	340.20	459.70	-	-
PCL	430.57	-	-	-	-

T_{max}: maximum degradation temperature.

Table 2. Endothermic events values for ATV, PCL, and PCL/ATV samples.

Samples	Events	Endothermic events						
		T onset/°C	1° Peak/°C	T end set/°C	ΔH_{fus}/J g^{-1}	T onset/°C	2°Peak °C	ΔH_{fus}/J g^{-1}
ATV	1	142.78	164.02	172.17	**64.210**	-	-	-
PCL	1	47.91	52.31	58.78	**61.676**	-	-	-
PA20	2	43.58	53.45	58.98	**58.090**	149.07	159.78	166.55
PA40	2	42.46	52.34	58.64	**49.256**	152.07	160.32	167.35
PA60	2	42.69	52.11	58.71	**44.862**	152.22	160.03	167.74
PA80	2	44.10	51.89	58.57	**40.602**	150.17	159.78	167.67

The PCL thermal degradation occurred in a single stage of mass loss. The onset was 390°C and the maximum thermal degradation occurred at 448°C (Table 1). This stage corresponds to the depolymerization of PCL from the ends of the polymer chain, with the hydroxyl terminal groups forming ε-caprolactone[23]. These results agree with the literature that described that PCL is completely decomposed in a single stage, with a peak of maximum degradation around 430°C[9,33].

As previously described[11,24], a five-stage weight loss was recorded for TGA curves. According to Shete et al.[2], the first phase of weight loss, around 80-140°C, is related to the loss of volatile that was absorbed on the surface. When adsorbed on the surface, water usually comes out at lower temperatures, around 60ºC, and, on the other hand, the connected water usually leaves around 100ºC. According to these authors, this result is consistent with the literature for ATV trihydrate[2]. In this work, stages of mass loss at 251ºC, 340ºC and 459ºC were observed for ATV. The theoretical value of mass loss for the trihydrate would be 4.46% and we observed a very close loss, 4.38%, indicating that this inference is probably correct[2]. It can also be observed in the TGA curve, that the greatest loss of volatile occurs after 200°C.

TGA analyze of PCL/ATV showed characteristics compatible with PCL and ATV. Table 1 shows the maximum temperatures observed in DTG curves (excluding the initial events at temperatures below 175°C) for both ATV, PCL, and PCL/ATV samples. These obtained results indicate that PCL/ATV samples showed intermediate characteristics between the curves of the drug and polymer in the thermal decomposition curves, indicating drug entrapment in the polymer matrix.

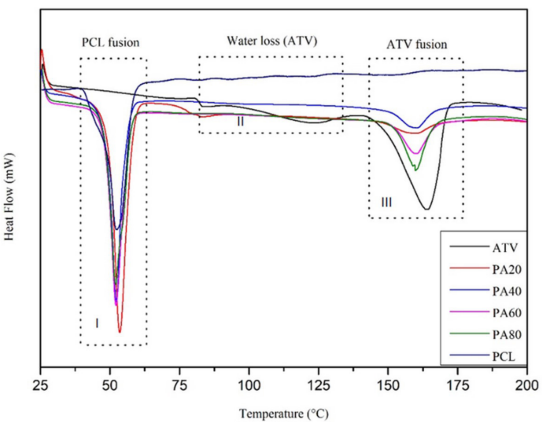

Figure 3. DSC curves of ATV and matrices- PCL (0 mg of ATV), PA20 (20 mg of ATV); PA40 (40 mg of ATV); PA60 (60 mg of ATV); PA80 (80 mg of ATV).

The DSC curves of ATV (Figure 4) present two endothermic events: one in the range of 80°C to 140ºC related to the loss of volatiles and the second around 160ºC due to the melting of ATV[32,34,35]. These results are consistent with the TGA data obtained in this work. The PCL matrix (Figure 3) showed a single endothermic peak that corresponds to the crystalline fusion at 52°C. A similar result was observed by Silva et al.[30], Sekosan and Vasanthan[36].

The peaks related to PCL fusion remained similar in the PCL/ATV samples. Nevertheless, since changes in the fusion enthalpy values were observed (Table 2) it is possible to infer

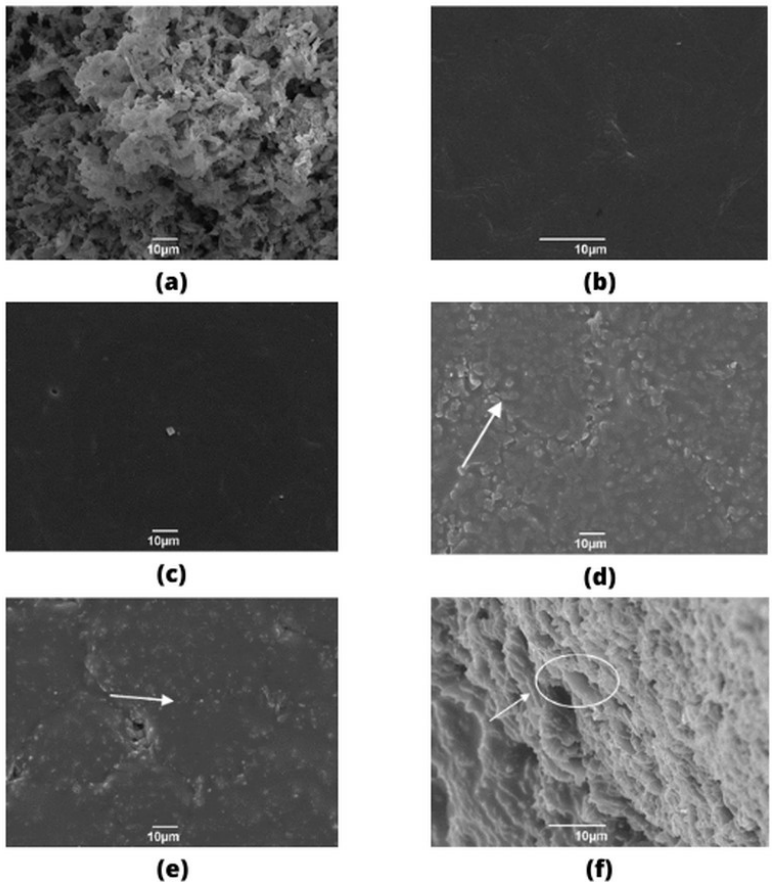

Figure 4. SEM images of the matrices: (a) ATV particles; (b) PCL matrices; (c) PA20; (d) PA40; (e) PA60 and (f) PA80.

that ATV alters the crystallinity of PCL (Figure 4). The value of ΔH decreases with increasing ATV content. This result agrees with the XRD analysis (Figure 2) that showed changes in the characteristic peak of the PCL. The peaks related to the drug and the amount of energy involved in thermal transitions were also modified. Considering the matrices, the endothermic events related to ATV were observed in PA40, PA60, and PA80 samples. Although, probably, due to the recrystallization of ATV in PCL, these peaks were shifted to higher temperatures (Table 2). In the PA20 sample, the peaks related to ATV were not observed, perhaps due to the low concentration of drug present in the sample

3.4. SEM and EDS Analysis

SEM images of ATV particles, PCL matrix, PA20, PA40, PA60, and PA80 matrices are shown in Figure 5. The ATV micrograph (Figure 4a) shows agglomerates of needle structures with variable length and width. The pure PCL matrix (Figure 4b) presented a smooth surface. According to SEM images (Figure 4c, 4d, 4e, and 4f), the morphology of the matrices was affected by the amount of ATV in the sample. Structures smaller than 10 µm can be observed on the surfaces of PA40 and PA60 matrices.

As mentioned, in the present work, ATV calcium was used. EDS analysis was performed to evaluate the calcium distribution on PA20 and PA40 surfaces (Figure 5). The EDS calcium map allows concluding that the drug is dispersed in the matrices and the clusters at the PA40 matrix are constituted by the drug (Figure 5b). This allows the extrapolation for the clusters observed in the SEM images of PA60 and PA80 (Figure 4e-4f) and the conclusion that these samples have excess particles on the surface, probably, outside the polymeric structure.

3.5. In vitro release study

PA60 and PA80 samples (Figure 6) were subjected to *in vitro* drug release studies. The films were produced in 3cm x 4cm molds and obtained thickness of 0.1cm.

ATV release was affected by its concentration in the sample as shown in Figure 7. During the studied period, it was observed that P60 (60 mg of ATV) and PA80 (80 mg of ATV) samples released 36,43% and 64,72% of ATV, respectively. The dissolution of the drug contained in the matrices can be considered prolonged because up to 15000 minutes it had not reached 100% release[37]. PCL is used in the development of controlled drug release systems due to its mechanical properties and these characteristics may have helped in the drug release behavior[9]. This result can be considered a positive one since one of the goals of this work was to produce ATV matrices with the prolonged release.

The experimental data were adjusted for the most used release models in the literature: zero-order kinetics, first-order

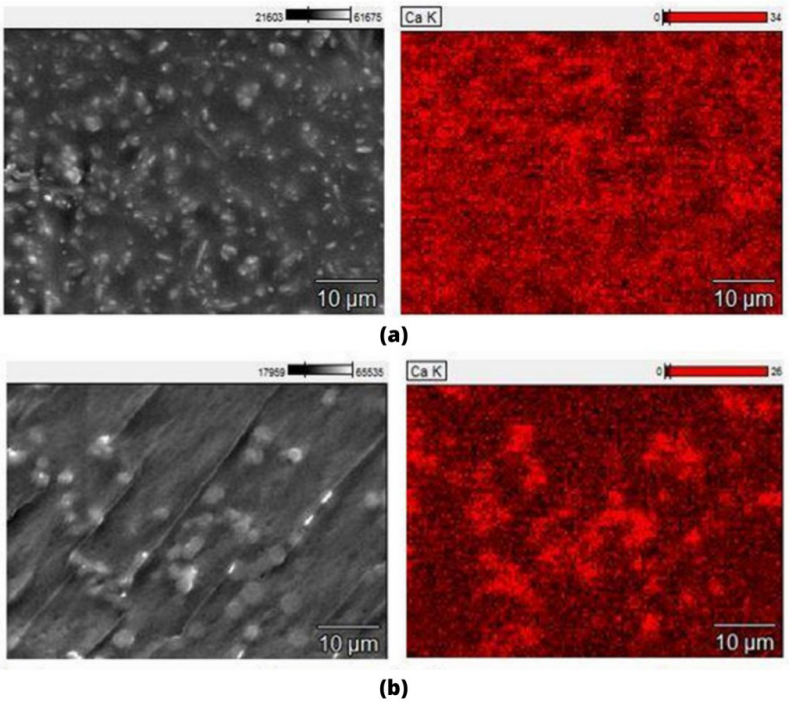

Figure 5. EDS analysis of the samples: (a) PA20 and (b) PA40.

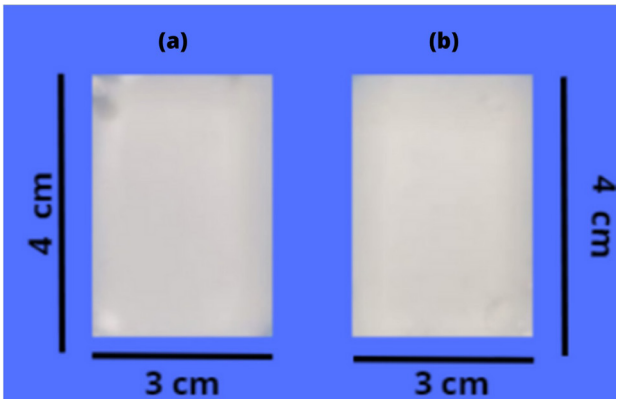

Figure 6. (a) PA60 and (b) PA80. Both films were produced in 3cm x 4cm molds and obtained thickness of 0.1 cm.

kinetics, Hixson-Crowell, Higuchi, Korsmeyer-Peppas and the correlation coefficients were determined. The values of the adjusted coefficients as well as the R^2 are presented in Table 3. According to the data, PA60 samples can be explained by the Hixson-Crowell and Higuchi model, being the last one which fits best (Table 3). In the PA80 sample, the kinetic release could be explained by kinetics model of order zero, Hixson-Crowell, Higuchi and Korsmeyer-Peppas model, the last one with the higher correlation coefficient (Table 3). This shows that more than one model can explain the initial drug release behavior. However, it is important to highlight that only the Higuchi model can be adjusted for both samples, since the R^2 values were above 0.96 for both.

Some considerations must be made for the application of the models. Higuchi's model, for example, is based

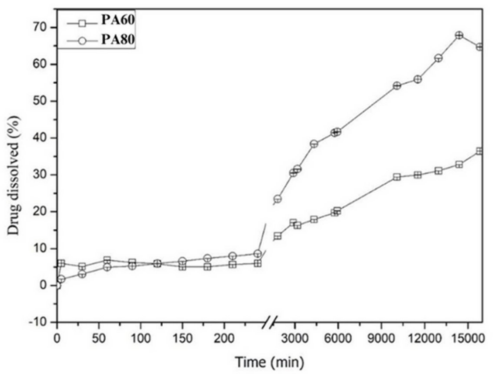

Figure 7. Dissolution profiles of PA60 (60 mg de ATV) e PA80 (80 mg de ATV) samples.

on Fick's law and in order to be used, it is necessary to consider different factors, such as: mass transport through the diffusion of the drug, being the limiting step; sink condition for ATV (which is poorly soluble in phosphate buffer pH 7.4[35]); the device must not be eroded while the drug is being delivered; the diffusion coefficient of the species must be constant; the swelling of the device must be insignificant or happen quickly in order to achieve balance; among others[37]. The dissolution process can change the matrices morphology and, consequently, the release behavior[38]. In fact, it is not, immediately, the erosion of the PCL itself, but the erosion of the matrix due to the exit of ATV. This erosion can create preferential pathways for the fluid.

To understand the effect of ATV's release from the matrix, SEM analysis of PA60 and PA80 samples after the release study was made and showed that erosion of the matrix occurred (Figure 8). In the images, it was possible to observe the formation of pores when compared to the micrographs before the release (Figure 4e-4f) , possibly due to the exit of the drug particles that were well incorporated in the matrices (PCL degradation can take 2 to 4 years depending on the initial molecular weight of the device or implant[9].

Nevertheless, the formation of pores in the matrix structure for tissue engineering could be positive, since it allows the initial fixation of cells, serving as a structure and allowing tissue regeneration[9,39]. In this context, these matrices produced by PCL and ATV start as a matrix of tissue and, as the release proceeds, there is the formation of pores that could facilitate tissue growth. Similar behavior was also seen by Jiao et al.[40] where the pore structure in the nano-hydroxyapatite (HA)/PCL and micro-HA/PCL tissue engineering scaffolds produced by 3D printing facilitated the growth of blood vessels, the transport of nutrients, and provided a very favorable environment for the discharge of cellular metabolic waste[40]. Also, in the work of Liu D. the 3D printed PCL/Strontium-HA bone scaffold was prepared with the aim of simulating the natural bone components, exhibiting significant osteogenic activity *in vitro* and *in vivo*, being able to simultaneously release strontium and calcium ions to promote osteogenesis repair due to its porosity[41].

According to the observation of SEM analysis about ATV release from matrices produced in this work, it is suggested that the mechanism of drug release from PA60 and PA80 samples occurs in the following steps:

(1) Solubilization of the drug particles that were closest to the sample surface.
(2) Diffusion of the drug particles that were inside the matrices structure into the solution, forming pores where previously were drug particles, which may cause the erosion of the polymer.
(3) Diffusion of the phosphate buffer solution into the matrix after the drug has started to dissolve, causing the swelling of the polymeric matrix and its erosion. Since PCL is hydrophobic, this process can be more difficult, being a factor with less impact on the release. These could explain the change in the release in the dissolution profile (Figure 8).

Table 3. Correlation coefficient models (zero-order kinetics, first-order kinetics, Hixson-Crowell, Higuchi and Korsmeyer-Peppas models) for the release kinetics of PA60 and PA80 samples.

Model	PA20	PA40
Zero-order kinetics	0,892	**0,943**
First-order kinetics	0,867	0,718
Hixson-Crowell	**0,939**	**0,963**
Higuchi	**0,969**	**0,969**
Korsmeyer-Peppas	0,844	**0,995**

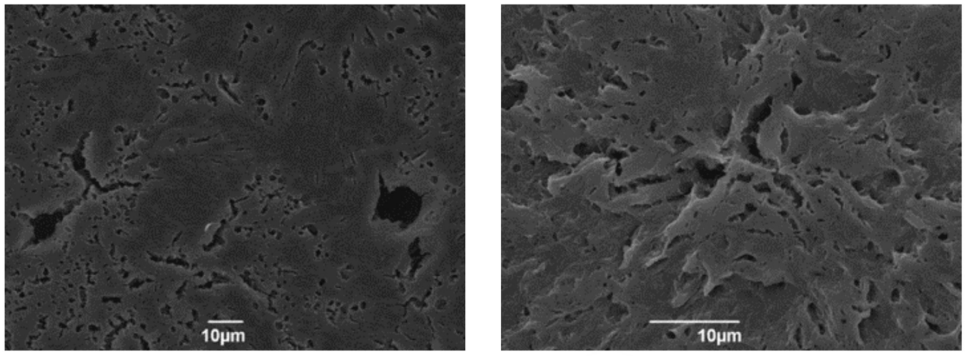

Figure 8. SEM images of matrices (a) PA20 and (b) PA40 after drug release (15000 minutes).

3. Conclusions

In the present work, PCL matrices containing ATV were obtained using the solvent casting method. The distribution of ATV in the matrices was uniform as observed in SEM analysis. All characterizations proved the incorporation of the drug in the matrices, maintaining its structure with minimal changes. It was observed that, at the end of the tests (after 15000 minutes), the obtained dissolution reached a maximum of 65%, indicating a prolonged release of the ATV, where the release process occurs in the following steps: solubilization of the drug on the matrix surface, diffusion of the drug from the matrices, and then erosion. The experimental data of the *in vitro* release analysis of the matrices were adjusted for different models and the one that showed the best fit for the two studied matrices was the Higuchi model, with a correlation coefficient above 0.95 for both. The conditions for the application of the Higuchi model were not completely satisfied in the present work, but, due to the obtained R^2 value, it is suggested that diffusion is an important step in the process of ATV release from PCL matrices produced by solvent casting.

4. References

1. Oliveira, LSAF, Oliveira CS, Machado APL, Rosa FP. Biomateriais com aplicação na regeneração óssea – método de análise e perspectivas futuras. Rev Ciênc Méd Biol. 2010;9(1):37. http://dx.doi.org/10.9771/cmbio.v9i1.4730.
2. Shete G, Puri V, Kumar L, Bansal AK. Solid state characterization of commercial crystalline and amorphous atorvastatin calcium samples. AAPS PharmSciTech. 2010;11(2):598-609. http://dx.doi.org/10.1208/s12249-010-9419-7.
3. Zhang HX, Wang JX, Zhang ZB, Le Y, Shen ZG, Chen JF. Micronization of atorvastatin calcium by antisolvent precipitation process. Int J Pharm. 2009;374(1-2):106-13. http://dx.doi.org/10.1016/j.ijpharm.2009.02.015.
4. Bone HG, Kiel DP, Lindsay RS, Lewiecki EM, Bolognese MA, Leary ET et al. Effects of atorvastatin on bone in postmenopausal women with dyslipidemia: a double-blind, placebo-controlled, dose-ranging trial. J Clin Endocrinol Metab. 2007;92(12):4671-7. http://dx.doi.org/10.1210/jc.2006-1909.
5. Zeybek ND, Gulcelik NE, Kaymaz FF, Sarisozen C, Vural I, Bodur E et al. Rosuvastatin induces apoptosis in cultured human papillary thyroid cancer cells. J Endocrinol. 2011;210(1):105-15. http://dx.doi.org/10.1530/JOE-10-0411.
6. Pasco JA, Kotowicz MA, Henry MJ, Sanders KM, Nicholson GC. Statin use, bone mineral density, and fracture risk. Arch Intern Med. 2002;162(5):537. http://dx.doi.org/10.1001/archinte.162.5.537.
7. Tai IC, Fu YC, Wang CK, Chang JK, Ho ML. Local delivery of controlled-release simvastatin/PLGA /HA p microspheres enhances bone repair. Int J Nanomedicine. 2013;8:3895-905. http://dx.doi.org/10.2147/IJN.S48694.
8. Kellesarian S, Al Amri M, Al-Kheraif A, Ghanem A, Malmstrom H, Javed F. Efficacy of local and systemic statin delivery on the osseointegration of implants: a systematic review. Int J Oral Maxillofac Implants. 2017;32(3):497-506. http://dx.doi.org/10.11607/jomi.4955.
9. Woodruff MA, Hutmacher DW. The return of a forgotten polymer - polycaprolactone in the 21st century. Prog Polym Sci. 2010;35(10):1217-56. http://dx.doi.org/10.1016/j.progpolymsci.2010.04.002.
10. Mendonça RH, Meiga TO, Costa MF, Thiré RMSM. Production of 3D scaffolds applied to tissue engineering using chitosan swelling as a porogenic agent. J Appl Polym Sci. 2013;129(2):614-25. http://dx.doi.org/10.1002/app.38735.
11. Pachuau L. Recent developments in novel drug delivery systems for wound healing. Expert Opin Drug Deliv. 2015;12(12):1895-909. https://doi.org/10.1517/17425247.2015.1070143.
12. Nafea EH, El-Massik MA, El-Khordagui LK, Marei MK, Khalafallah NM. Alendronate PLGA microspheres with high loading efficiency for dental applications. J Microencapsul. 2007;24(6):525-38. http://dx.doi.org/10.1080/02652040701439807.
13. Miladi K, Sfar S, Fessi H, Elaissari A. Enhancement of alendronate encapsulation in chitosan nanoparticles. J Drug Deliv Sci Technol. 2015;30:391-6. http://dx.doi.org/10.1016/j.jddst.2015.04.007.
14. Posadowska U, Parizek M, Filova E, Wlodarczyk-Biegun M, Kamperman M, Bacakova L et al. Injectable nanoparticle-loaded hydrogel system for local delivery of sodium alendronate. Int J Pharm. 2015;485(1-2):31-40. http://dx.doi.org/10.1016/j.ijpharm.2015.03.003.
15. Rong HJ, Chen WL, Guo SR, Lei L, Shen YY. PCL films incorporated with paclitaxel/5-fluorouracil: effects of formulation and spacial architecture on drug release. Int J Pharm. 2012;427(2):242-51. http://dx.doi.org/10.1016/j.ijpharm.2012.02.007.
16. Khunová V, Kováčová M, Olejniková P, Ondreáš F, Špitalský Z, Ghosal K et al. Antibacterial electrospun polycaprolactone nanofibers reinforced by halloysite nanotubes for tissue engineering. Polymers. 2022;14(4):746. http://dx.doi.org/10.3390/polym14040746.
17. Ghosal K, Chandra A, Praveen G, Snigdha S, Roy S, Agatemor C et al. Electrospinning over solvent casting: tuning of mechanical properties of membranes. Sci Rep. 2018;8(1):5058. http://dx.doi.org/10.1038/s41598-018-23378-3.
18. McCullen SD, Autefage H, Callanan A, Gentleman E, Stevens MM. Anisotropic fibrous scaffolds for articular cartilage regeneration. Tissue Eng Part A. 2012;18(19-20):2073-83. http://dx.doi.org/10.1089/ten.tea.2011.0606.
19. Şaşmazel HT, Gümüşderelioğlu M, Gürpınar A, Onur MA. Comparison of cellular proliferation on dense and porous PCL scaffolds. Biomed Mater Eng. 2016;18(3):119-28. https://doi.org/10.3233/BME-2008-0515.
20. Tang ZG, Black RA, Curran JM, Hunt JA, Rhodes NP, Williams DF. Surface properties and biocompatibility of solvent-cast poly[ε-caprolactone] films. Biomaterials. 2004;25(19):4741-8. http://dx.doi.org/10.1016/j.biomaterials.2003.12.003.
21. Sinha VR, Bansal K, Kaushik R, Kumria R, Trehan A. Poly-ϵ-caprolactone microspheres and nanospheres: an overview. Int J Pharm. 2004;278(1):1-23. https://doi.org/10.1016/j.ijpharm.2004.01.044.
22. Salmoria GV, Cardenuto MR, Roesler CRM, Zepon KM, Kanis LA. PCL/Ibuprofen implants fabricated by selective laser sintering for orbital repair. Procedia CIRP. 2016;49:188-92. http://dx.doi.org/10.1016/j.procir.2015.11.013.
23. Williams JM, Adewunmi A, Schek RM, Flanagan CL, Krebsbach PH, Feinberg SE et al. Bone tissue engineering using polycaprolactone scaffolds fabricated via selective laser sintering. Biomaterials. 2005;26(23):4817-27. http://dx.doi.org/10.1016/j.biomaterials.2004.11.057.
24. Barrère F, Mahmood TA, Groot K, Van Blitterswijk CA. Advanced biomaterials for skeletal tissue regeneration: instructive and smart functions. Mater Sci Eng Rep. 2008;59:38-71. http://dx.doi.org/10.1016/j.mser.2007.12.001.
25. Beier F. Cholesterol and cartilage do not mix well. Nat Rev Rheumatol. 2019;15(5):253-4. http://dx.doi.org/10.1038/s41584-019-0204-z.
26. Choi WS, Lee G, Song WH, Koh JT, Yang J, Kwak JS et al. The CH25H–CYP7B1–RORα axis of cholesterol metabolism regulates osteoarthritis. Nature. 2019;566:254-8. http://dx.doi.org/10.1038/s41586-019-0920-1.

27. Bruschi ML, editor. Strategies to modify drug release from pharmaceutical systems. Cambridge: Elsevier; 2015. https://doi.org/10.1016/C2014-0-02342-8.
28. Costa P, Lobo JMS. Modeling and comparison of dissolution profiles. Eur J Pharm Sci. 2001;13(2):123-33. https://doi.org/10.1016/s0928-0987(01)00095-1.
29. Gómez-Lizárraga KK, Flores-Morales C, Prado-Audelo ML, Álvarez-Pérez MA, Piña-Barba MC, Escobedo C. Polycaprolactone- and polycaprolactone/ceramic-based 3D-bioplotted porous scaffolds for bone regeneration: a comparative study. Mater Sci Eng C. 2017;79:326-35. http://dx.doi.org/10.1016/j.msec.2017.05.003.
30. Silva EP, Pereira MAV, Lima IPB, Lima NGPB, Barbosa EG, Aragão CFS et al. Compatibility study between atorvastatin and excipients using DSC and FTIR. J Therm Anal Calorim. 2016;123(2):933-9. http://dx.doi.org/10.1007/s10973-015-5077-z.
31. Tower CW, Allen K, Carandang A, Van Horn RM. Solubility considerations in relative block crystallization and morphology of PEO-*b*-PCL films. Polym Cryst. 2020;3(3):e10107. https://doi.org/10.1002/pcr2.10107.
32. Choudhary A, Rana AC, Aggarwal G, Kumar V, Zakir F. Development and characterization of an atorvastatin solid dispersion formulation using skimmed milk for improved oral bioavailability. Acta Pharm Sin B. 2012;2(4):421-8. http://dx.doi.org/10.1016/j.apsb.2012.05.002.
33. Fukushima K, Tabuani D, Camino G. Nanocomposites of PLA and PCL based on montmorillonite and sepiolite. Mater Sci Eng C. 2009;29(4):1433-41. http://dx.doi.org/10.1016/j.msec.2008.11.005.
34. Jahangiri A, Barzegar-Jalali M, Garjani A, Javadzadeh Y, Hamishehkar H, Afroozian A et al. Pharmacological and histological examination of atorvastatin-PVP K30 solid dispersions. Powder Technol. 2015;286:538-45. http://dx.doi.org/10.1016/j.powtec.2015.08.047.
35. Sonje VM, Kumar L, Meena CL, Kohli G, Puri V, Jain R et al. Atorvastatin calcium. In: Brittain HG, editor. Profiles of drug substances, excipients and related methodology. Amsterdam: Elsevier; 2010. Vol. 35; p. 1-70. https://doi.org/10.1016/S1871-5125(10)35001-1.
36. Sekosan G, Vasanthan N. Morphological changes of annealed poly-ε-caprolactone by enzymatic degradation with lipase. J Polym Sci B Polym Phys. 2010;48(2):202-11. http://dx.doi.org/10.1002/polb.21889.
37. Adepu S, Ramakrishna S. Controlled drug delivery systems: current status and future directions. Molecules. 2021;26:5905. http://dx.doi.org/10.3390/molecules26195905.
38. Ren J. Biodegradable poly(lactic acid): synthesis, modification, processing and applications. Berlin: Springer; 2010. Application in the field of biomedical materials; p. 240-72. https://doi.org/10.1007/978-3-642-17596-1_7.
39. Hutmacher DW, Schantz T, Zein I, Ng KW, Teoh SH, Tan KC. Mechanical properties and cell cultural response of polycaprolactone scaffolds designed and fabricated via fused deposition modeling. J Biomed Mater Res A. 2001;55(2):203-16. http://dx.doi.org/10.1002/1097-4636(200105)55:2<203:AID-JBM1007>3.0.CO;2-7.
40. Jiao Z, Luo B, Xiang S, Ma H, Yu Y, Yang W. 3D printing of HA / PCL composite tissue engineering scaffolds. Adv Indus Eng Polym Res. 2019;2(4):196-202. http://dx.doi.org/10.1016/j.aiepr.2019.09.003.
41. Liu D, Nie W, Li D, Wang W, Zheng L, Zhang J et al. 3D printed PCL/SrHA scaffold for enhanced bone regeneration. Chem Eng J. 2019;362:269-79. http://dx.doi.org/10.1016/j.cej.2019.01.015.